Journal of *Marine Science and Engineering*

MDPI

Article

Development of Recovery System for Underwater Glider

Thinh Huynh [1,†], Minh-Thien Tran [2,†], Munhaeng Lee [3], Young-Bok Kim [3,4], Jungwoo Lee [4,5] and Jin-Ho Suh [3,4,*]

[1] Department of Chassis and Body, Ho Chi Minh City University of Technology and Education, Ho Chi Minh City 70000, Vietnam
[2] Industrial Science Technology Research Center, Major of Mechanical System Engineering, Pukyong National University, Busan 48513, Korea
[3] Department of Intelligent Robot Engineering, Pukyong National University, Busan 48513, Korea
[4] Major of Mechanical System Engineering, Division of Energy Transport Systems Engineering, Pukyong National University, Busan 48513, Korea
[5] Smart Mobility Research Center, Korea Institute of Robotics and Technology Convergence (KIRO), Pohang 37666, Korea
* Correspondence: suhgang@pknu.ac.kr
† These authors contributed equally to this work.

Abstract: This study proposes a novel autonomous system that is able to retrieve an underwater glider safely and quickly. After a long-period mission, the glider is out of its energy, floats up in the middle of the sea, and needs retrieval. However, most of the recovery processes are conducted manually, which is not effective and even damages the glider or injures the worker. In this study, we propose the use of a remotely operated vehicle (ROV) in a recovery process that consists of three stages: (i) driving the ROV into the near area of the glider, (ii) automatically catching the glider using the ROV's onboard sensors and capturing mechanisms, and (iii) retrieving the glider to the mother ship or station. Mathematical models were formulated to realize the feasibility of the system. A cascade adaptive sliding mode control-proportional integral controller is designed to cope with the thruster's characteristics, the dynamics of the ROV and the glider, and oceanic disturbances. Finally, simulation studies were conducted in the system operation scenarios and their results validate the efficiency of the proposed process.

Keywords: underwater glider; glider recovery; remotely operated vehicle (ROV); cascade control; adaptive sliding mode control

check for updates

Citation: Huynh, T.; Tran, M.-T.; Lee, M.; Kim, Y.-B.; Lee, J.; Suh, J.-H. Development of Recovery System for Underwater Glider. *J. Mar. Sci. Eng.* **2022**, *10*, 1448. https://doi.org/10.3390/jmse10101448

Academic Editor: Hugo Guterman

Received: 14 September 2022
Accepted: 5 October 2022
Published: 7 October 2022

Publisher's Note: MDPI stays neutral with regard to jurisdictional claims in published maps and institutional affiliations.

Copyright: © 2022 by the authors. Licensee MDPI, Basel, Switzerland. This article is an open access article distributed under the terms and conditions of the Creative Commons Attribution (CC BY) license (https://creativecommons.org/licenses/by/4.0/).

1. Introduction

Nowadays, the use of ocean data is becoming popular in marine engineering and ecosystem management. Thanks to this information, complex tasks such as typhoon prediction, whale ecological monitoring, and red tide monitoring can be conducted reliably. In order to collect the necessary oceanographic data, underwater gliders carrying multiple instruments and communication systems have been developed and deployed. The gliders are a type of non-holonomic autonomous underwater vehicle (AUV) that employs buoyancy propulsions instead of propellers or thrusters. By switching between negative and positive buoyancies, the gliders follow an up-and-down sawtooth-like trajectory very slowly but consume very little energy. Therefore, they offer a significantly greater range and endurance. Hence, they are able to perform ocean sampling missions from hours to weeks or months, and to thousands of kilometers of range [1–3]. After these long-period missions, the gliders float up in the middle of the sea, are unable to return by themselves, and required retrieving. In other cases, such as a glider being damaged or drifting out of its planned trajectory, rescue missions are also required. Unfortunately, recovering a glider is always a challenging task.

The conventional approach is to use human skills and rudimentary equipment, such as nets, cranes, belts, and hooks, to bring back a glider, as depicted in Figure 1. For example, the Argo project [4,5] comprises 3000 underwater gliders scattered throughout the world's oceans. To recover a glider to check and calibrate it before the next mission, a mother ship approached the location the glider had sent. The worker dropped the net below and then pulled it towards the glider so that the glider fits in the net. The two were then lifted by a crane, and workers used their strength to pull them back to the mother ship. The succession of the work relies on the experience and skills of the operators. Moreover, the glider may collide with the ship and recovery equipment such that its body and instruments take damage. In bad weather conditions, not only does the retrieving task become more difficult, but the risk of accidents to people also increases. Therefore, a safe and automatic glider recovery method is necessary.



Figure 1. The manual recovery of underwater gliders.

On the other hand, numerous projects have been conducted on recovery AUVs, which have a similar structure and dynamical characteristics to the glider. A favorite recovery method is to control the AUV to dock into a capture mechanism such as a funnel, net, and pole [6–9]. The docking procedure is generally as follows: the AUV follows a global path to approach the station; determines the location and posture of the dock station; generates the docking path; and finally, follows the guidance and enters the docking cabin. The docking process is possible thanks to the maneuverability of a traditional AUV. Unfortunately, for the non-holonomic AUVs, the docking maneuver is more challenging. The complexity of the maneuver and the influence of the turbulence environment cause the docking process to fail easily and damage the AUV. Especially for an uncontrollable glider after its mission, the process is not possible. Several studies designed a docking cabin that is movable by being carried by a submarine [10] or surface vehicle [11]. However, the succession of docking still relies on the AUV's motion performance.

Then comes the use of other types of vehicles to retrieve an AUV; some still require a certain level of operation of the AUV, while others just control the retrieving vehicle without controlling the AUV. Multi-propeller aerial vehicles have been deployed in [12] for not only recovery but also deployment of the AUVs. The recovery mechanism first uses a line and hook and then evolves by utilizing an electro-permanent magnet to capture and release the AUV. The line and hook put risk on both vehicles, but the other mechanism shows its capability. However, the airflow generated by the propellers creates large turbulence over the water and disturbs the position of the vehicle to be recovered. Remotely operated vehicles (ROVs) were used to recover submerged vehicles in [13,14]. The ROVs were equipped with a camera and a gripper so that their operator can search and capture the submerged assets remotely. Unfortunately, it was difficult for the operator to estimate the position and the distance between the two vehicles from the camera's perspective. Sarda et al. [15,16] designed an AUV recovery system based on unmanned surface vehicles. The recovery involves lowering a thin line with an outrigger-type depressor wing from the winch on the surface vehicle, latching the line with the AUV using a pincer-type onboard mechanism, and finally, reeling the line for vehicle retrieval. For the process, the

AUV has to be submerged underwater. Moreover, lining up the recovery mechanism is not easily done with only the controlled motion of the surface vehicles. Thus, different mechanisms are designed and examined, such as funnel recovery [17], and wing and rope capturing [18] devices.

Due to its great potential, surface vehicle-based systems have been considered for glider recovery; for example, in the study of Howse et al. [9]. Since the glider floats on the surface of the ocean, which is different from the AUV, the surface vehicle is designed with the Small Waterplane Area Twin Hull (SWATH) form. The recovery mechanism uses a net with linkages helping it catch and lift the glider in a similar way to the manual operation. Hence, disadvantages of manual operation remain, such as the risk of damaging the glider and the difficulty of controlling the recovery system. Other approaches require modifying significantly the glider [19–21] such that it has autonomous recovery capability. Apparently, it cannot recover itself when running out of energy. Nevertheless, very few studies have considered the problem of automatic glider recovery in our knowledge. The process still heavily relies on manual operation, which is full of risks and drawbacks.

Therefore, in this study, we propose a novel glider recovery method using a ROV. The vehicle is renovated with additional instruments and mechanisms for the objective of capturing and retrieving the glider. The recovery process consists of three stages: (i) driving the ROV to the neighborhood area below the glider, (ii) determining the position and orientation of the glider and catching it, and (iii) retrieving the glider to the mother ship or station. In order to analyze the maneuverability of the recovery system, the mathematical model is firstly derived, and a cascade adaptive sliding mode control (ASMC)-proportional integral (PI) control system is then designed. Simulation studies in the operation scenario of the system show its feasibility. Comparison results with a cascade proportional integral derivative (PID)-PI also validate the effectiveness of the proposed system. Then, the contributions of this paper can be summarized as follows:

- A novel recovery method for the underwater glider using the ROV is proposed.
- The mathematical model of the ROV is derived while taking the process (dynamics of the recovered glider, hydrodynamics, buoyancy effects, etc.) into the formulation
- The cascade ASMC-PI control system is designed. The system stability is proved by the Lyapunov-like lemma. The system's effectiveness and robustness are validated through comparative simulations.

The remainder of the paper is organized into 5 sections. Section 2 introduces the proposed glider recovery process. The mathematical model of the system is derived in Section 3. The design of the cascade ASMC-PI control system is presented in detail in Section 4, whereas its control performance is discussed in Section 5. Finally, conclusions are drawn in Section 6.

2. Proposed Glider Recovery Process

In this study, the propeller-type ROV is used to recover the target underwater glider. For this objective, the ROV first needs to determine the position and posture of the glider. We place a stereo camera in the front of the ROV, and the lighting system ensures we can obtain good vision even when submerging. Numerous studies proposed reliable methods to detect and estimate the posture of an object with this visual data, for example in [22–25]. The ROV also uses the sensors such as an inertial measurement unit (IMU) and global positioning system (GPS) to measure its own position and rotation. The ROV is equipped with a gripper and a clamp for capturing and carrying the glider. The gripper picks up the hook underneath the glider, which is a minor accessory added to the glider. The clamp is kept fully opening while the ROV is deployed from the mother ship or operating station. After picking up, the ROV adjusts its posture so that the clamp holds tightly the upper body of the glider when closing up. Then, the glider moves together with the ROV and is retrieved. The structure of the renovated ROV is depicted in Figure 2.

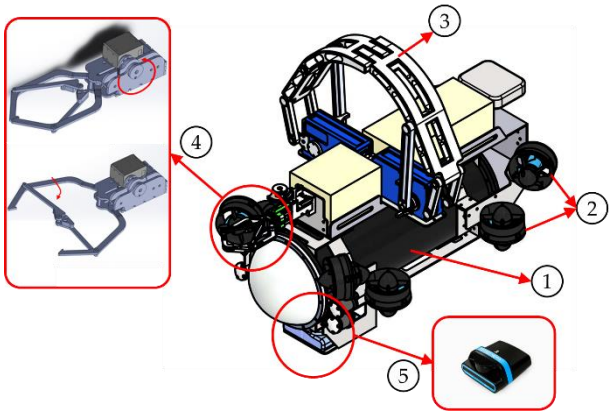
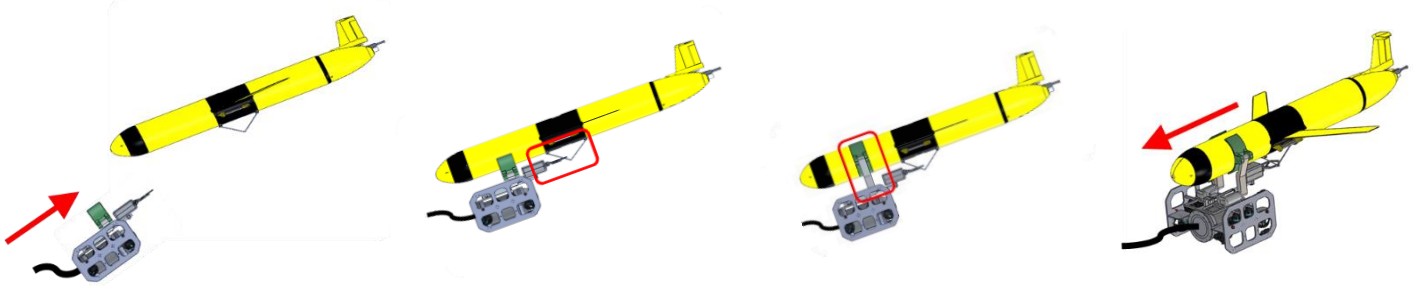


Figure 2. The proposed ROV for retrieving the underwater glider. (1) Main body; (2) Thrusters; (3) Clamp; (4) Gripper; (5) Stereo camera.

With this ROV, the proposed glider recovery process involves three stages:

Approaching stage: After localizing the glider to be recovered, the ROV is deployed from the mother ship or operating station. It follows a global trajectory, avoids obstacles, and avoids colliding with the glider's body. The ROV reaches a destination point below the glider, points toward it, and then switches to the next stage.

Capturing stage: Through the visual data obtained from the stereo camera, the position and orientation of the glider in the ROV-fixed coordinates are determined. A path planning algorithm, for example [26], generates the required movements for the ROV, including the movement to the pick-up point for the gripper and the subsequent rotation to a position parallel to the glider. The posture estimation and path planning tasks are conducted similarly to those in the docking operations mentioned in the literature review. The difference is that those tasks are conducted by the ROV instead of the vehicle to be recovered. The ROV performs the motion as follows: (i) It follows the guidance to the pick-up point for the gripper; (ii) the gripper catches the hook beneath the glider; (iii) the ROV rotates following the given guidance; and (iv) the clamp holds the upper body of the glider. These motions are illustrated in Figure 3.



(**a**) (**b**) (**c**) (**d**)

Figure 3. The capturing stage of the proposed process: (**a**) The ROV approaches the glider from below; (**b**) The ROV's gripper picks up the hook on the glider's body; (**c**) The ROV's clamp holds the glider's body; (**d**) The ROV starts to retrieve the glider back to a mother ship or station.

Retrieving stage: The ROV carries the glider back to the mother ship or station.

It is worth noting the second stage requires completely autonomous operation. This is due to the close distance between two vehicles, thus resulting in a high precision requirement. Besides, an operator has the difficulty in estimating the absolute position and the depth from the camera perspective. The motion path in other stages can be either remotely given by the operator or automatically generated by the path planning algorithm. The control system has to give an effective and robust performance in the whole process.

3. System Modeling

In order to analyze the maneuverability of the recovery system, the system dynamics are formulated. We consider the motions in three coordinates: the Earth-fixed frame (or inertial frame) XYZ, the ROV's body-fixed frame $X_bY_bZ_b$ and the glider-fixed frame $X_gY_gZ_g$. They are depicted in Figure 4. Key dimensions of the ROV, as well as the actuating thrust forces, are also shown in the figure.

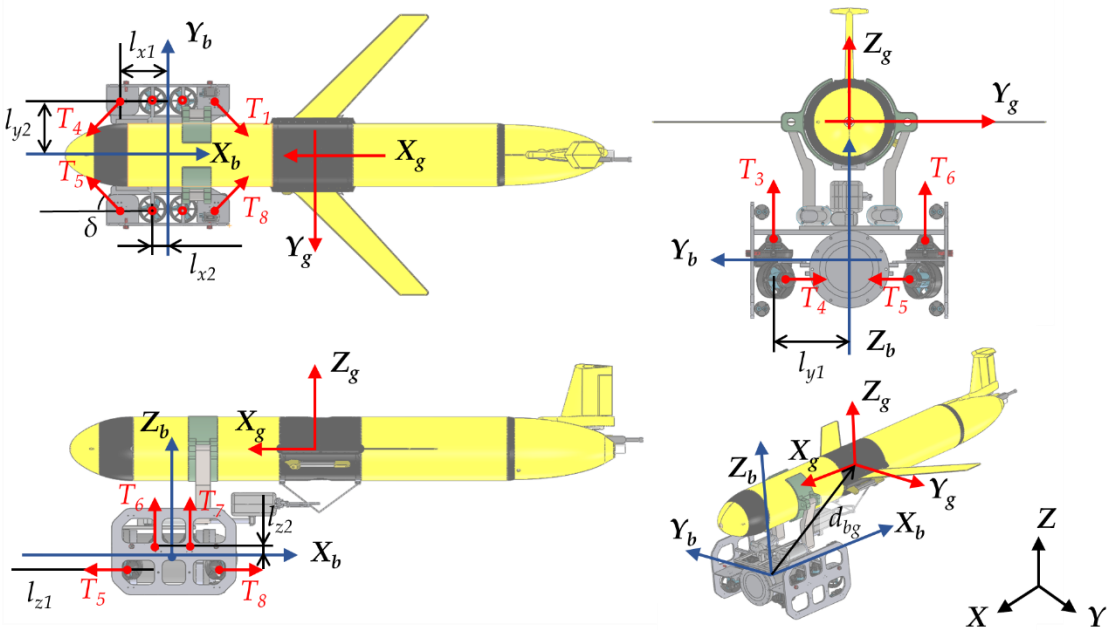


Figure 4. Schematic drawing of the glider recovery system using the ROV.

The rigid-body dynamics of the ROV submerged in water, including hydrodynamic drag and added mass parameters, are as follows [27,28]:

$$\begin{aligned} \dot{\boldsymbol{\eta}} &= \boldsymbol{J}(\boldsymbol{\eta})\boldsymbol{\nu}, \\ \boldsymbol{M}\dot{\boldsymbol{\nu}} &= -\boldsymbol{C}(\boldsymbol{\nu})\boldsymbol{\nu} - \boldsymbol{D}(\boldsymbol{\nu})\boldsymbol{\nu} - \boldsymbol{g}(\boldsymbol{\eta}) + \boldsymbol{\tau} + \boldsymbol{\tau}_C + \boldsymbol{\tau}_G \end{aligned} \tag{1}$$

where:

$\boldsymbol{\eta} = \begin{bmatrix} x & y & z & \phi & \theta & \psi \end{bmatrix}^T$ is the vector containing the position and the orientation of the body frame with respect to the Earth-fixed frame. The orientation is represented by three Euler angles of roll, pitch, and yaw in XYZ order.

$\boldsymbol{\nu} = \begin{bmatrix} u & v & w & p & q & r \end{bmatrix}^T$ is the state vector of body-frame linear and angular velocities.

$\boldsymbol{J}(\boldsymbol{\eta})$ is the transformation matrix from the body frame to the inertial frame. It is given by:

$$\begin{aligned} \boldsymbol{J}(\boldsymbol{\eta}) &= \begin{bmatrix} \boldsymbol{R}_B^I & \boldsymbol{O}_3 \\ \boldsymbol{O}_3 & \boldsymbol{J}_{k,o}^{-1} \end{bmatrix}, \\ \boldsymbol{R}_B^I &= \begin{bmatrix} c_\psi c_\theta & s_\psi c_\theta & -s_\theta \\ -s_\psi c_\phi + c_\psi s_\theta s_\phi & c_\psi c_\theta + s_\psi s_\theta s_\phi & s_\phi c_\theta \\ s_\psi s_\phi + c_\psi s_\theta c_\phi & -c_\psi s_\phi + s_\psi s_\theta c_\phi & c_\phi c_\theta \end{bmatrix}^{-1}, \quad \boldsymbol{J}_{k,o}^{-1} = \frac{1}{c_\theta} \begin{bmatrix} c_\theta & s_\phi s_\theta & c_\phi s_\theta \\ 0 & c_\phi c_\theta & -s_\phi c_\theta \\ 0 & s_\phi & c_\phi \end{bmatrix} \end{aligned} \tag{2}$$

with $c_{(\cdot)} = \cos(\cdot)$ and $s_{(\cdot)} = \sin(\cdot)$.

$\boldsymbol{M}$ denotes the matrix of the ROV's mass and inertia including added mass and inertia parameters due to hydrodynamic effects. The matrix is diagonal if the origin of the

body-fixed frame is chosen coincident with the central frame and the body is completely submerged in the water, the velocity is low, and it has three planes of symmetry.

$$\begin{aligned} \boldsymbol{M} &= \boldsymbol{M}_{AUV} + \boldsymbol{M}_A, \\ \boldsymbol{M}_{AUV} &= \begin{bmatrix} m\boldsymbol{I}_3 & \boldsymbol{O}_3 \\ \boldsymbol{O}_3 & \boldsymbol{J} \end{bmatrix}, \\ \boldsymbol{M}_A &= -diag\left(X_{\dot{u}}, Y_{\dot{v}}, Z_{\dot{w}}, K_{\dot{p}}, M_{\dot{q}}, N_{\dot{r}}\right) \end{aligned} \tag{3}$$

where m and $\boldsymbol{J}$ are the ROV's own mass and inertia tensor. $diag(X_{\dot{u}}, Y_{\dot{v}}, Z_{\dot{w}})$ contains the added mass and $diag\left(K_{\dot{p}}, M_{\dot{q}}, N_{\dot{r}}\right)$ is the added inertial. $\boldsymbol{O}_3$ and $\boldsymbol{I}_3$ are the 3-by-3 zeros and identity matrices, respectively.

$\boldsymbol{C}(\boldsymbol{\nu})$ is the nonlinear Coriolis and centripetal matrix. As in [27,28], $\boldsymbol{C}(\boldsymbol{\nu})$ is introduced as follows:

$$\boldsymbol{C}(\boldsymbol{\nu}) = \boldsymbol{C}_{AUV}(\boldsymbol{\nu}) + \boldsymbol{C}_A(\boldsymbol{\nu}),$$

$$\boldsymbol{C}_{AUV}(\boldsymbol{\nu}) = \begin{bmatrix} 0 & 0 & 0 & 0 & mw & -mv \\ 0 & 0 & 0 & -mw & 0 & mu \\ 0 & 0 & 0 & mv & -mu & 0 \\ 0 & mw & -mv & 0 & J_z r & -J_y q \\ -mw & 0 & mu & -J_z r & 0 & J_x p \\ mv & -mu & 0 & J_y q & -J_x p & 0 \end{bmatrix}, \quad \boldsymbol{C}_A(\boldsymbol{\nu}) = \begin{bmatrix} 0 & 0 & 0 & 0 & -Z_{\dot{w}} w & Y_{\dot{v}} v \\ 0 & 0 & 0 & Z_{\dot{w}} w & 0 & -X_{\dot{u}} u \\ 0 & 0 & 0 & -Y_{\dot{v}} v & X_{\dot{u}} u & 0 \\ 0 & -Z_{\dot{w}} w & Y_{\dot{v}} v & 0 & -N_{\dot{r}} r & M_{\dot{q}} q \\ Z_{\dot{w}} w & 0 & -X_{\dot{u}} u & Y_{\dot{v}} v & 0 & -K_{\dot{p}} p \\ -Y_{\dot{v}} v & X_{\dot{u}} u & 0 & -M_{\dot{q}} q & K_{\dot{p}} p & 0 \end{bmatrix} \tag{4}$$

The diagonal, linear, and quadratic hydrodynamic drag matrix is denoted by $\boldsymbol{D}(\boldsymbol{\nu})$ and they are given by:

$$\boldsymbol{D}(\boldsymbol{\nu}) = -diag\left(X_u, Y_v, Z_w, K_p, M_q, N_r\right) - diag\left(X_{u|u|}|u|, Y_{v|v|}|v|, Z_{w|w|}|w|, K_{p|p|}|p|, M_{q|q|}|q|, N_{r|r|}|r|\right) \tag{5}$$

with the coefficients of $\boldsymbol{D}(\boldsymbol{\nu})$ being considered to be constant.

$\boldsymbol{g}(\boldsymbol{\eta})$ is the restoring force and moment vector that combines gravitational and buoyancy effects. In the ROV's body-fixed frame, the ROV's center of gravity is at $r_G^B = \begin{bmatrix} 0 & 0 & 0 \end{bmatrix}^T$ and its center of buoyancy is at $r_B^B = \begin{bmatrix} x_B & y_B & z_B \end{bmatrix}^T$. Then, the restoring force and moment vector is obtained by:

$$\boldsymbol{g}(\boldsymbol{\eta}) = \begin{bmatrix} (m - \rho\nabla) g s_\theta \\ -(m - \rho\nabla) g c_\theta s_\phi \\ -(m - \rho\nabla) g c_\theta c_\phi \\ \rho\nabla g\left(y_B c_\theta c_\phi - z_B c_\theta s_\phi\right) \\ \rho\nabla g\left(-z_B s_\theta - x_B c_\theta c_\phi\right) \\ \rho\nabla g\left(x_B c_\theta s_\phi + y_B s_\theta\right) \end{bmatrix} \tag{6}$$

In which, g is the gravitational acceleration, ρ is the water density, and ∇ the volume of the body underwater.

The vector of control force and moment is denoted by $\boldsymbol{\tau}$ and resulted from the thrust vector $\boldsymbol{T}$ generated by the thruster assembly. From the configuration of the thrusters shown in Figure 4, $\boldsymbol{\tau}$ relates to the thrusts via the thruster configuration matrix as follows:

$$\boldsymbol{\tau} = \boldsymbol{K_T T},$$

$$\boldsymbol{T} = \begin{bmatrix} T_1 & T_2 & T_3 & T_4 & T_5 & T_6 & T_7 & T_8 \end{bmatrix}^T,$$

$$\boldsymbol{K_T} = \begin{bmatrix} c_\delta & 0 & 0 & -c_\delta & -c_\delta & 0 & 0 & c_\delta \\ -s_\delta & 0 & 0 & -s_\delta & s_\delta & 0 & 0 & s_\delta \\ 0 & 1 & 1 & 0 & 0 & 1 & 1 & 0 \\ -l_{z1} s_\delta & l_{y2} & l_{y2} & -l_{z1} s_\delta & l_{z1} s_\delta & -l_{y2} & -l_{y2} & l_{z1} s_\delta \\ -l_{z1} c_\delta & -l_{x2} & l_{x2} & l_{z1} c_\delta & l_{z1} c_\delta & l_{x2} & -l_{x2} & -l_{z1} c_\delta \\ -l_{x1} s_\delta - l_{y1} c_\delta & 0 & 0 & l_{x1} s_\delta + l_{y1} c_\delta & -l_{x1} s_\delta - l_{y1} c_\delta & 0 & 0 & l_{x1} s_\delta + l_{y1} c_\delta \end{bmatrix} \tag{7}$$

In addition, the dynamics of the thrusters generate thrust is assumed to follow the hydrodynamic linear model [29]. For the ith thruster, the model is presented by:

$$\begin{aligned} \dot{n}_i &= -k_{1i}n_i - k_{2i}Q_i(n_i, v_i) + k_{3i}u_i, \\ \dot{v}_i &= -k_{4i}(v_i - U)|v_i - U| + k_{5i}T_i(n_i, v_i), \\ T_i(n_i, v_i) &= c^T_{n_i}n_i|n_i| - c^T_{n_iv_i}|n_i|v_i, \\ Q_i(n_i, v_i) &= c^Q_{n_i}n_i|n_i| - c^Q_{n_iv_i}|n_i|v_i \end{aligned} \tag{8}$$

where n_i and v_i are the ith propeller angular velocity and the axial fluid velocity, respectively. $T_i(n_i, v_i)$ and $Q_i(n_i, v_i)$ represent its thrust output and reaction torque. U is the ambient velocity. k_{ji} (j = 1,2,3,4) are positive definite, so are the parameters $c^T_{n_i}$, $c^T_{n_iv_i}$, $c^Q_{n_i}$ and $c^Q_{n_iv_i}$. Additionally, u_i is the actuator's voltage to be controlled.

Moreover, the effects of waves, wind, and, especially, ocean currents are denoted by $\boldsymbol{\tau_C}$. By assuming the current irrotational and constant in the earth-fixed frame, its effects can be modeled as follows:

$$\boldsymbol{\tau}_C = -\begin{bmatrix} \boldsymbol{R}^B_I & \boldsymbol{O}_3 \\ \boldsymbol{O}_3 & \boldsymbol{R}^B_I \end{bmatrix} \boldsymbol{\theta}_{vC} \tag{9}$$

with $\boldsymbol{\theta}_{vC}$ the vector of constant parameters contributing to the earth-fixed generalized forces and moments due to the current.

Finally, $\boldsymbol{\tau}_G$ is the vector of resistance force and moment from the glider acting on the ROV. That means before retrieving the glider, $\boldsymbol{\tau}_G = 0$, and after the ROV catches the glider, $\boldsymbol{\tau}_G$ is resultant from the glider motion. The latter case is formulated by:

$$\begin{aligned} \boldsymbol{\tau}_G &= -\boldsymbol{K}_G\left(\boldsymbol{M}_G\dot{\boldsymbol{\nu}} + \boldsymbol{C}_G(\boldsymbol{\nu})\boldsymbol{\nu} + \boldsymbol{D}_G(\boldsymbol{\nu})\boldsymbol{\nu} + \boldsymbol{g}_G(\boldsymbol{\eta}) - \boldsymbol{\tau}_{GC}\right), \\ \boldsymbol{K}_G &= \begin{bmatrix} \boldsymbol{I}_3 & \boldsymbol{O}_3 \\ \boldsymbol{S}(\boldsymbol{d}_{bg}) & \boldsymbol{I}_3 \end{bmatrix} \end{aligned} \tag{10}$$

where $\boldsymbol{d}_{bg} = \begin{bmatrix} d_x & d_y & d_z \end{bmatrix}^T$ is the vector of translation from the origin of the ROV's body-fixed frame to the mass center of the glider. $\boldsymbol{S}(\boldsymbol{d}_{bg})$ denotes the skew-symmetrical matrix of $\boldsymbol{d}_{bg}$. $\boldsymbol{M}_G$, $\boldsymbol{C}_G(\boldsymbol{\nu})$, and $\boldsymbol{D}_G(\boldsymbol{\nu})$ are, respectively, the mass and inertia matrix, the Coriolis and centripetal matrix, and the drag matrix of the glider. Finally, $\boldsymbol{g}_G(\boldsymbol{\eta})$ and $\boldsymbol{\tau}_{GC}$ are the forces and moments acting on the glider and are modeled in a similar manner to those of the ROV. It is noted that since the glider is tightly held by the ROV, its translational and rotational velocities in the ROV's body-fixed frame is the same as those of the ROV.

On the other hand, it is worth noting that in the second stage of the glider recovery process, both the position and orientation of the glider are required to be measured so that the glider can be captured successfully. In other words, the representation of the glider-fixed frame relative to the ROV's body-fixed frame must be obtained. Moreover, if one can derive the position in this frame of at least three certain points of the glider, the relative position and orientation of the glider are completely defined. This is done using the stereo camera system in this study. Figure 5 illustrates the 6-dimensional pose estimation of the glider in this stage using the stereo camera system on the ROV, in which the position of a point A on the glider's body expressed in the ROV's body-fixed frame is computed by:

$$\begin{aligned} \begin{bmatrix} x^B_A & y^B_A & z^B_A \end{bmatrix}^T &= \begin{bmatrix} d^B_C + d_A & l^B_{C_1} + l_{A1} & h^B_C + h_A \end{bmatrix}^T, \\ d_A = \frac{l_C f}{-x^{C_1}_A S^{C_1}_x + x^{C_2}_A S^{C_2}_x}, \quad l_{A1} &= -d_A\frac{x^{C_1}_A S^{C_1}_x}{f}, \quad h_A = -\frac{y^{C_1}_A S^{C_1}_y}{f d_A} \end{aligned} \tag{11}$$

where $x^{C_1}_A$ and $y^{C_1}_A$ represent the projection of A on the horizontal and vertical coordinates, respectively, of the image plane of the right camera (camera C_1). $S^{C_1}_x$ and $S^{C_1}_y$ are the horizontal and vertical size of a pixel. f denotes the focal length and $\begin{bmatrix} d^B_C & l^B_{C_1} & h^B_C \end{bmatrix}^T$ is the

location of camera C_1 in the ROV's body-fixed frame. Finally, l_C is the distance between the two cameras in the stereo camera system.

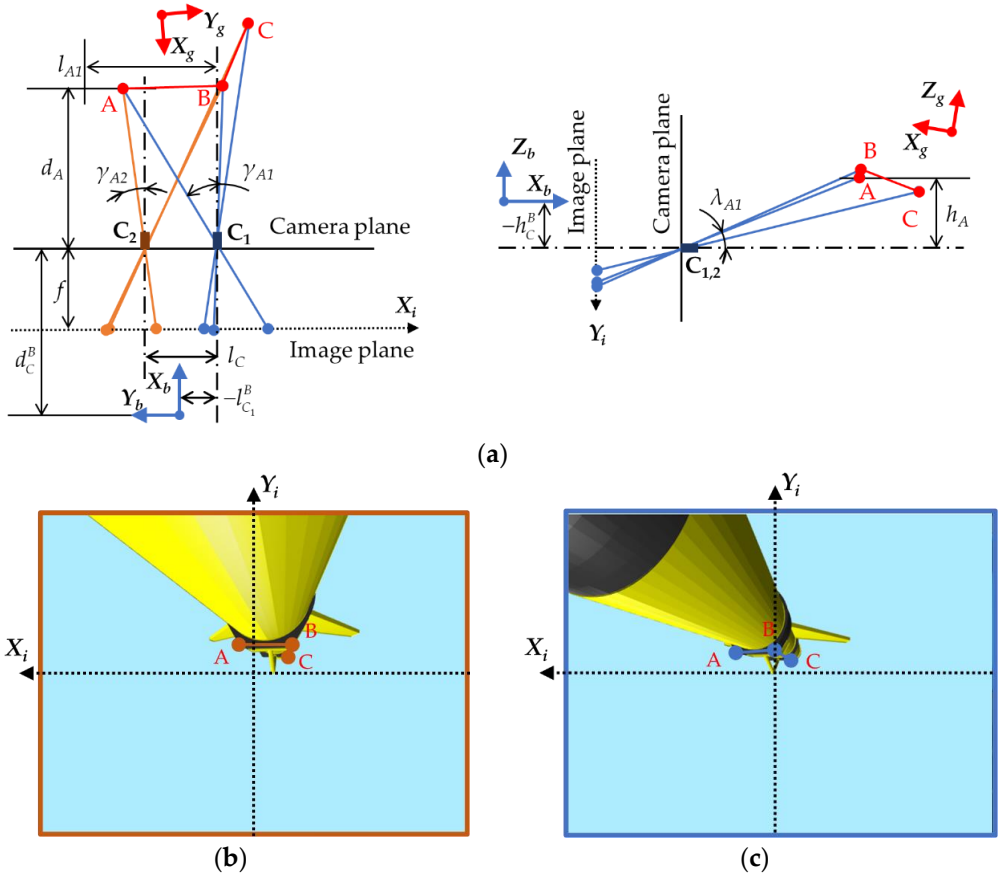


Figure 5. A 6-dimensional pose estimation of the glider in the capturing stage: (**a**) Schematic drawing of the measurement using the stereo camera; (**b**) projected points in the left image (camera C_2); (**c**) projected points in the right image (camera C_1).

4. Motion Control System Design

The objective of the motion control system is to operate the ROV's thrusters such that the ROV follow the desired paths of motion, both before and after retrieving the glider. In practical operations, the desired paths are given by an operator, in the case of remote control of the ROV, or from a motion planning algorithm based on the position of the glider and the measurement system equipped in the ROV. To fulfill the control objective, a cascade control structure is proposed. In the outer control loop, the sliding mode control law computes the force and moment for the ROV to reach its desired motion. In the inner loop, each thruster is controlled by the PI controller such that it generates thrust as required. In order to effectively cope with disturbances and uncertainties, an adaptive law is added to the control system.

Assume that the voltage input of each thruster can be mapped to its generated thrust such that $T_i = K_{ui}u_i$. Then to the total force and moment acting on the ROV. This can be done by either a variety of models, such as linear gains or nonlinear dead-zone functions [30,31], or experimental tests. Then, the dynamics model of AUV in Equation (1) can be rearranged as follows:

$$\begin{aligned} \dot{\boldsymbol{\eta}} &= \boldsymbol{J}_B^I(\boldsymbol{\eta})\boldsymbol{\nu}, \\ \boldsymbol{M}\dot{\boldsymbol{\nu}} &= -\boldsymbol{C}(\boldsymbol{\nu})\boldsymbol{\nu} - \boldsymbol{D}(\boldsymbol{\nu})\boldsymbol{\nu} - \boldsymbol{g}(\boldsymbol{\eta}) + \boldsymbol{\tau}_u + \boldsymbol{\tau}_{u,d} + \boldsymbol{\tau}_C + \boldsymbol{\tau}_G \end{aligned} \tag{12}$$

where $\boldsymbol{\tau_u}$ is the vector of force and moment mapped from the thrusters' voltage input $\boldsymbol{u}$. $\boldsymbol{\tau_{u,d}}$ is the remaining dynamical terms between $\boldsymbol{\tau}$ and $\boldsymbol{u}$. Let us assume that these dynamics can be approximated by first-order models. Moreover, Equation (12) can be rewritten entirely in the Earth-fixed frame, to eliminate the terms expressed in the body-fixed frame, as follows [27,28,32,33]:

$$\boldsymbol{M_\eta}\ddot{\boldsymbol{\eta}} + \left(\boldsymbol{\Lambda_\eta} + \Delta\boldsymbol{\Lambda_\eta}\right)\dot{\boldsymbol{\eta}} + \boldsymbol{g_\eta}(\boldsymbol{\eta}) + \boldsymbol{d_\tau} = \boldsymbol{\tau_{u,\eta}} \tag{13}$$

In which:

$$\begin{gathered} \boldsymbol{M_\eta} = \left(\boldsymbol{J_B^I}(\boldsymbol{\eta})\right)^{-T}\boldsymbol{M}\left(\boldsymbol{J_B^I}(\boldsymbol{\eta})\right)^{-1}, \\ \boldsymbol{\Lambda_\eta} + \Delta\boldsymbol{\Lambda_\eta} = \boldsymbol{C_\eta}(\boldsymbol{\nu},\boldsymbol{\eta}) + \boldsymbol{D_\eta}(\boldsymbol{\nu},\boldsymbol{\eta}), \\ \boldsymbol{d_\tau} = -\boldsymbol{\tau_{C,\eta}} - \boldsymbol{\tau_{G,\eta}} - \boldsymbol{\tau_{u,d,\eta}} \end{gathered} \tag{14}$$

and

$$\begin{gathered} \boldsymbol{C_\eta}(\boldsymbol{\nu},\boldsymbol{\eta}) = \left(\boldsymbol{J_B^I}(\boldsymbol{\eta})\right)^{-T}\left(\boldsymbol{C}(\boldsymbol{\nu}) - \boldsymbol{M}\left(\boldsymbol{J_B^I}(\boldsymbol{\eta})\right)^{-1}\dot{\boldsymbol{J}}_{\boldsymbol{B}}^{\boldsymbol{I}}(\boldsymbol{\eta})\right)\left(\boldsymbol{J_B^I}(\boldsymbol{\eta})\right)^{-1}, \\ \boldsymbol{D_\eta}(\boldsymbol{\nu},\boldsymbol{\eta}) = \left(\boldsymbol{J_B^I}(\boldsymbol{\eta})\right)^{-T}\boldsymbol{D}(\boldsymbol{\nu})\left(\boldsymbol{J_B^I}(\boldsymbol{\eta})\right)^{-1},\ \boldsymbol{g_\eta}(\boldsymbol{\eta}) = \left(\boldsymbol{J_B^I}(\boldsymbol{\eta})\right)^{-T}\boldsymbol{g}(\boldsymbol{\eta}), \\ \boldsymbol{\tau_{u,d,\eta}} = \left(\boldsymbol{J_B^I}(\boldsymbol{\eta})\right)^{-T}\boldsymbol{\tau_{u,d}},\ \boldsymbol{\tau_{C\eta}} = \left(\boldsymbol{J_B^I}(\boldsymbol{\eta})\right)^{-T}\boldsymbol{\tau_C},\ \boldsymbol{\tau_{G\eta}} = \left(\boldsymbol{J_B^I}(\boldsymbol{\eta})\right)^{-T}\boldsymbol{\tau_G},\ \boldsymbol{\tau_{u,\eta}} = \left(\boldsymbol{J_B^I}(\boldsymbol{\eta})\right)^{-T}\boldsymbol{\tau_u} \end{gathered} \tag{15}$$

The term $\boldsymbol{\Lambda_\eta}$ represents the nominal value of $\boldsymbol{C_\eta}(\boldsymbol{\nu},\boldsymbol{\eta}) + \boldsymbol{D_\eta}(\boldsymbol{\nu},\boldsymbol{\eta})$, and $\Delta\boldsymbol{\Lambda_\eta}$ denotes the remaining uncertainty. The uncertainty $\Delta\boldsymbol{\Lambda_\eta}$ and the disturbance $\boldsymbol{d_\tau}$ are assumed to be bounded and satisfy the matching condition.

For a given vector $\boldsymbol{\eta_d}$ of the desired position and orientation of the ROV in the Earth-fixed frame, let the tracking error be defined as $\boldsymbol{e}=\boldsymbol{\eta} - \boldsymbol{\eta_d}$. A vector of sliding surfaces is considered as follows:

$$\boldsymbol{s}=\dot{\boldsymbol{e}}+\boldsymbol{K_s}\boldsymbol{e} \tag{16}$$

With $\boldsymbol{K_s}$ a positive diagonal matrix. $\boldsymbol{s}$ converges to zero equivalent to the asymptotic stability of the ROV.

From Equations (13)–(16), the following dynamics of the sliding surfaces is obtained:

$$\begin{gathered} \dot{\boldsymbol{s}}=\boldsymbol{M_\eta^{-1}}\left(\boldsymbol{\tau_{u,\eta}} - \boldsymbol{\Lambda_\eta}\dot{\boldsymbol{\eta}} - \boldsymbol{g_\eta}(\boldsymbol{\eta})\right) - \ddot{\boldsymbol{\eta}}_{\boldsymbol{d}} + \boldsymbol{K_s}\dot{\boldsymbol{e}} + \boldsymbol{D_e}\left(\dot{\boldsymbol{\eta}},\boldsymbol{\tau}\right), \\ \boldsymbol{D_e}\left(\dot{\boldsymbol{\eta}},\boldsymbol{\tau}\right) = \boldsymbol{M_\eta^{-1}}\left[-\Delta\boldsymbol{\Lambda_\eta}\dot{\boldsymbol{\eta}} - \boldsymbol{d_\tau}\right] \end{gathered} \tag{17}$$

$\boldsymbol{D_e}\left(\dot{\boldsymbol{\eta}},\boldsymbol{\tau}\right)$ denotes the total effect of the uncertainties and disturbances on the sliding surface. In order to guarantee that the sliding variable converges to zero, even with the presence of uncertainties and disturbances, the ASMC control law is proposed in the following form:

$$\boldsymbol{\tau_{u,\eta}} = \boldsymbol{\tau_o}+\boldsymbol{\tau_{a*}} \tag{18}$$

$\boldsymbol{\tau_o}$ is the equivalent control input and $\boldsymbol{\tau_{a*}}$ is the switching adaptation input. In our proposed control law, $\boldsymbol{\tau_o}$ is designed to achieve the convergence of the nominal sliding surface, i.e., the surface without uncertainties and disturbances. Therefore:

$$\boldsymbol{\tau_o} = \boldsymbol{M_\eta^{-1}}\ddot{\boldsymbol{\eta}}_{\boldsymbol{d}} + \boldsymbol{\Lambda_\eta}\dot{\boldsymbol{\eta}} + \boldsymbol{g_\eta}(\boldsymbol{\eta}) - \boldsymbol{M_\eta^{-1}}\boldsymbol{K_s}\dot{\boldsymbol{e}} \tag{19}$$

Meanwhile, each element of the adaptation term $\boldsymbol{\tau_{a*}}$ is designed as follows:

$$\begin{gathered} \tau_{ai} = -\hat{\omega}_{ai}\mathrm{sgn}(s_i), \\ \dot{\hat{\omega}}_{ai} = \alpha_i|s_i| \end{gathered} \tag{20}$$

In which, τ_{ai} and s_i, $(i = 1, 2, \ldots, 6)$, are the *ith* elements of the vector $\boldsymbol{\tau_{a*}}$ and $\boldsymbol{s}$, respectively. α_i is the corresponding positive adaptation gain. Assume that there exists a positive ω_{di} is a terminal solution that is greater than the boundedness of the corresponding

element d_{ei} of $\boldsymbol{D_e}(\dot{\boldsymbol{\eta}}, \boldsymbol{\tau})$. To validate the stability of the system controlled by the above ASMC law, we examine the following Lyapunov-like function candidate:

$$V = \frac{1}{2}\boldsymbol{s}^T\boldsymbol{s} + \frac{1}{2}\sum_{i=1}^{6}\frac{(\hat{\omega}_{ai} - \omega_{di})^2}{\alpha_i} \tag{21}$$

Taking the time derivative of (21) yields the following result:

$$\begin{aligned}\dot{V} &= \boldsymbol{s}^T\dot{\boldsymbol{s}} + \sum_{i=1}^{6}\frac{(\hat{\omega}_{ai}-\omega_{di})}{\alpha_i}\dot{\hat{\omega}}_{ai} \\ &= \sum_{i=1}^{6}|s_i|(d_{ei}\mathrm{sgn}(s_i) - \omega_{di}) < 0\end{aligned} \tag{22}$$

Hence, the derivative of the Lyapunov function candidate (21) is negative definite. Based on Barbalat's Lemma [34], the global stability of the ROV's motion is preserved.

In addition, the PI control laws are implemented to compensate for the thrusters' dynamics. From the desired force and moment, $\boldsymbol{\tau_{u,\eta}}$ obtained from the ASMC loop and their actual values $\boldsymbol{\tau_u}$, the ROV's force and moment vector is commanded as follows:

$$\begin{aligned}\boldsymbol{\tau_{u,PI}} &= \boldsymbol{K_{PT}}\boldsymbol{e_\tau} + \boldsymbol{K_{IT}}\int_0^t \boldsymbol{e_\tau}dt, \\ \boldsymbol{e_\tau} &= \boldsymbol{\tau_{u,\eta}} - \boldsymbol{\tau_u}\end{aligned} \tag{23}$$

where, $\boldsymbol{K_{PT}}$ and $\boldsymbol{K_{IT}}$ are the proportional and integral gains of the controller, respectively. Finally, we derive the voltage input for each thruster:

$$\begin{aligned}\boldsymbol{T} &= \boldsymbol{K_T^T}\left(\boldsymbol{K_T}\boldsymbol{K_T^T}\right)^{-1}\boldsymbol{\tau_{u,PI}}, \\ u_i &= \frac{1}{K_{ui}}T_i\end{aligned} \tag{24}$$

The schematic drawing of the proposed control system is depicted in Figure 6 below.

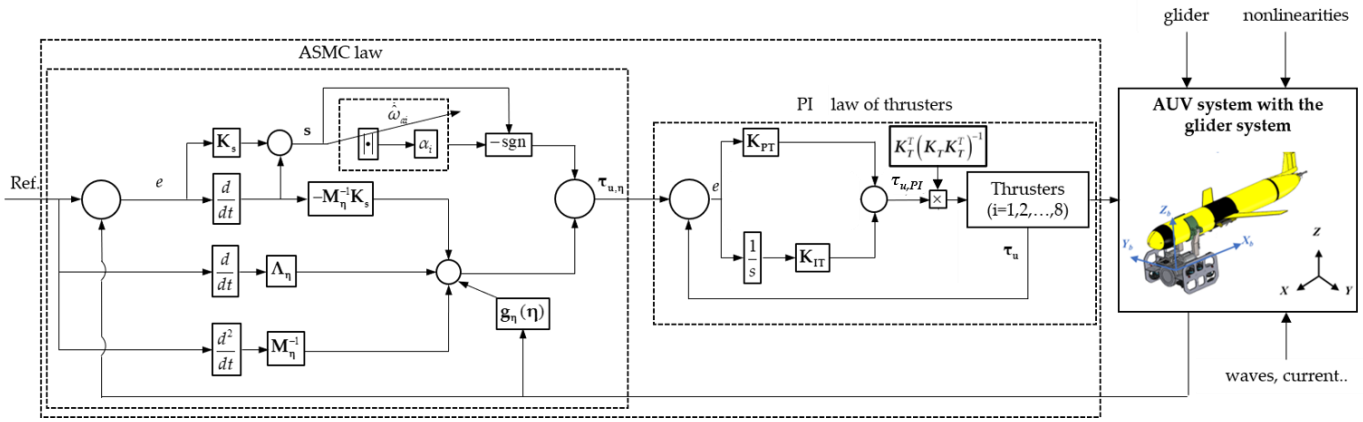


Figure 6. The proposed cascade ASMC-PI control law for the ROV retrieving the underwater glider.

5. Simulation Results and Discussion

5.1. Simulation Setup

In this simulation study, we examine the motion control performance of the system. The simulation scenario is illustrated in Figure 7 and consists of the first and final stages of the recovery process. In the approaching stage, the ROV is deployed from the mother ship or operating station on the water surface. It dives into the water and then tracks a curvature trajectory to the below the glider. The glider is located at $\begin{bmatrix}8 & 6 & 0\end{bmatrix}^T$[m] with respect to the initial location of the ROV. This stage consumes 80 [s] to finish. In a completed process, the

ROV then performs the capturing stage, which is fundamentally a tracking task in a similar manner to the previous stage. Thus, we neglect it in the simulation. In the final stage, the ROV retrieves the glider back. The retrieving path can be simply a straight line since there is no concern about colliding with the glider as in the capturing stage. In other words, the desired trajectory in the simulation is given by:

$$\boldsymbol{\eta}_d(t) = \begin{cases} \frac{x^2}{25} + \frac{y^2}{25} + \frac{z^2}{r_d^2} = 1 \text{ if } t \leq 80 \ [s], \\ y = \frac{4}{3}x, \ z = 0 \quad \text{otherwise} \end{cases} \tag{25}$$

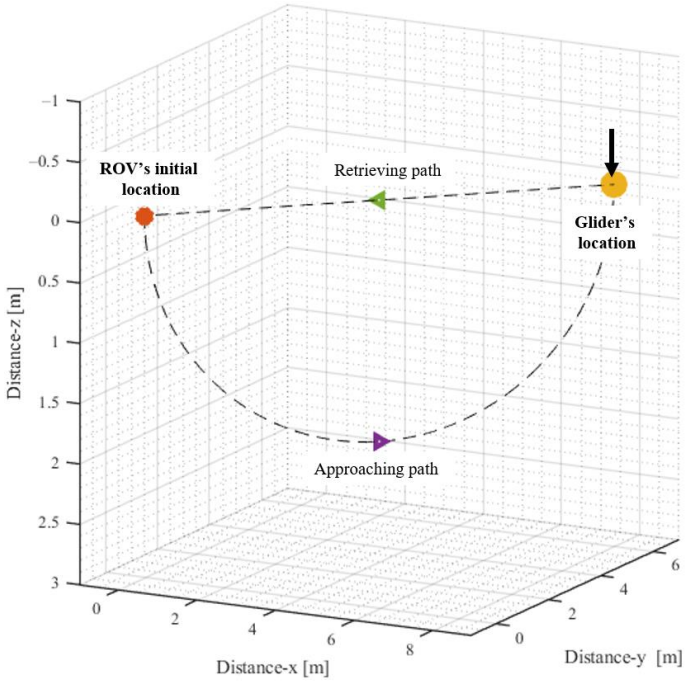


Figure 7. The simulation scenario.

The physical parameters of ROV in this simulation are given in Tables 1–5 and referred to in [35]. The parameters of the thruster models are experimentally obtained in [29] and shown in Table 6. The total effect of waves, wind, and ocean currents is defined through $\boldsymbol{\theta}_{vC} = [0.15\,[\text{N}] \ \ 0.35\,[\text{N}] \ \ 0.8\,[\text{N}] \ \ 0.02\,[\text{Nm}] \ \ 0.05\,[\text{Nm}] \ \ 0.07\,[\text{Nm}]]^T$. The influence of the retrieval glider is treated as additive resistance forces and moments in the latter part of the simulation. In this paper, we assume the effect of the glider is a constant $\boldsymbol{\tau}_G = [20.3\,[\text{N}] \ \ 20.3\,[\text{N}] \ \ 20.3\,[\text{N}] \ \ 5.6\,[\text{Nm}] \ \ 7.6\,[\text{Nm}] \ \ 10.3\,[\text{Nm}]]^T$. The other disturbances are also added to the scenario to validate the robustness of the control system. They are given by:

$$\boldsymbol{\tau}_d = [2.3\sin 0.4t\,[\text{N}] \ \ 1.5\sin 0.8t\,[\text{N}] \ \ 4\sin 0.7t\,[\text{N}] \ \ 0.15\sin 0.1t\,[\text{Nm}] \ \ 0.1\sin 0.4t\,[\text{Nm}] \ \ 0.2\sin 0.5t\,[\text{Nm}]]^T \tag{26}$$

Table 1. The hydrodynamic parameters.

$X_u = -72\,\text{kg.s}^{-1}$	$X_{\dot{u}} = -29\,\text{kg}$	$X_{u\|u\|} = 0\,\text{kg.m}^{-1}$
$Y_v = -77\ \text{kg.s}^{-1}$	$Y_{\dot{v}} = -30\ \text{kg}$	$Y_{v\|v\|} = 0\ \ \text{kg.m}^{-1}$
$Z_w = -95\,\text{kg.s}^{-1}$	$Z_{\dot{w}} = -90\,\text{kg}$	$Z_{w\|w\|} = 0\,\text{kg.m}^{-1}$
$K_p = -40\ \text{kg.m.s}^{-1}$	$K_{\dot{p}} = -5.2\,\text{kg.m}$	$K_{p\|p\|} = 0\ \text{kg.m}^{-1}$
$M_q = -30\,\text{kg.m.s}^{-1}$	$M_{\dot{q}} = -7.2\,\text{kg.m}$	$M_{q\|q\|} = 0\,\text{kg.m}^{-1}$
$N_r = -30\,\text{kg.m.s}^{-1}$	$N_{\dot{r}} = -3.3\,\text{kg.m}$	$N_{r\|r\|} = 0\ \text{kg.m}^{-1}$

Table 2. The moments of inertia.

$I_{xx} = 1.32\,\text{kg.m}^2$	$I_{xy} = I_{xz} = 0\,\text{kg.m}^2$
$I_{yy} = 2.08\,\text{kg.m}^2$	$I_{yx} = I_{yz} = 0\,\text{kg.m}^2$
$I_{zz} = 2.32\,\text{kg.m}^2$	$I_{zx} = I_{zy} = 0\,\text{kg.m}^2$

Table 3. The center of gravity and buoyancy.

$x_G = 0\,\text{m}$	$x_B = 0\,\text{m}$
$y_G = 0\,\text{m}$	$y_B = 0\,\text{m}$
$z_G = 0\,\text{m}$	$z_B = -0.05\,\text{m}$

Table 4. The underwater vehicles' parameters.

$\rho = 1028.48\,\text{kg.m}^3$
$\nabla = 0.09577\,\text{m}^3$
$g = 9.81\,\text{m.s}^{-2}$

Table 5. The thrusters' configuration parameters.

$\delta = \frac{\pi}{4}\,\text{rad}$	$l_{x2} = 0.15\,\text{m}$
$l_{x1} = 0.5\,\text{m}$	$l_{y2} = 0.5\,\text{m}$
$l_{y1} = 0.5\,\text{m}$	$l_{z2} = 0.2\,\text{m}$
$l_{z1} = 0.2\,\text{m}$	

Table 6. The parameters of the thruster hydrodynamic linear models.

$\boldsymbol{k}_1 = 13.66[1\ 1\ 1\ 1\ 1\ 1]^T\ \text{s}^{-1}$	$\boldsymbol{c}_n^T = 0.001467[1\ 1\ 1\ 1\ 1\ 1]^T\ \text{N.s}^2$
$\boldsymbol{k}_2 = 1856[1\ 1\ 1\ 1\ 1\ 1]^T\ (\text{N.m.s}^2)^{-1}$	$\boldsymbol{c}_{nv}^T = 0.4146[1\ 1\ 1\ 1\ 1\ 1]^T\ \text{N.s}^2\text{.m}^{-1}$
$\boldsymbol{k}_3 = 117.97[1\ 1\ 1\ 1\ 1\ 1]^T\ \text{m}(\text{N.s}^2)^{-1}$	$\boldsymbol{c}_n^Q = 2.804 \times 10^{-6}[1\ 1\ 1\ 1\ 1\ 1]^T\ \text{N.s}^2\text{.m}^{-2}$
$\boldsymbol{k}_4 = 1.102[1\ 1\ 1\ 1\ 1\ 1]^T\ \text{s}^{-1}$	$\boldsymbol{c}_{nv}^Q = 1.296 \times 10^{-11}[1\ 1\ 1\ 1\ 1\ 1]^T\text{N.s}^2$
$\boldsymbol{k}_5 = 0.01232[1\ 1\ 1\ 1\ 1\ 1]^T\ \text{m}(\text{N.s}^2)^{-1}$	$\boldsymbol{U} = 0.35[1\ 1\ 1\ 1\ 1\ 1]^T\ \text{m.s}^{-1}$

For the sake of validation, a cascade PID-PI control system is taken into comparison with our proposed ASMC-PI. Their parameters are listed in Table 7.

Table 7. The controllers' gains.

Outer loop	ASMC	$\boldsymbol{K_s} = diag(11.50,\ 6.81,\ 7.52,\ 16.51,\ 11.52,\ 14.11)$, $\boldsymbol{\alpha} = diag(28.51,\ 32.18,\ 5.27,\ 7.12,\ 8.32,\ 14.12)$
	PID	$\boldsymbol{K_P} = diag(145,\ 200,\ 183,\ 84,\ 40,\ 50)$, $\boldsymbol{K_I} = diag(140,\ 230,\ 180,\ 32,\ 25,\ 25)$, $\boldsymbol{K_D} = diag(106,\ 170,\ 350,\ 82,\ 74,\ 60)$
Inner loop	PI	$\boldsymbol{K_{PT}} = diag(0.85,\ 0.99,\ 0.6,\ 0.15,\ 0.1,\ 0.89)$, $\boldsymbol{K_{IT}} = diag(15,\ 5.1,\ 10,\ 15,\ 10,\ 16.1)$

5.2. Motion Performance in the Approaching Stage

The tracking performance of the ROV in 3D geometry is illustrated in Figure 8 and the tracking error in each direction with respect to time is shown in Figure 9. Both controllers are able to maneuver the ROV following the desired trajectory, but the proposed cascade ASMC-PI controller performs better. Although the proposed controller seems to give a larger fluctuation than the PID controller at the beginning, the tracking errors in Figure 9 show that only the motion in the z-direction is the case. The deviation in the z-direction motion quickly converges in 20 [s] and remains in a neighbor of zero after that. In comparison, the

PID-PI controlled system had a smaller tracking error in this direction at the beginning. However, it is unable to compensate effectively for the error and results in fluctuation in the whole period. Better performances of the proposed control system are easily seen in every other direction. The voltage inputs in Figure 10 show that the ASMC-PI controller quickly adjusts the operation of each thruster such that high-precision tracking is achieved. Especially when the ROV reaches the end of the first stage, it is close to the glider. Thus, deviation from the tracking trajectory may lead to a collision between the two vehicles.

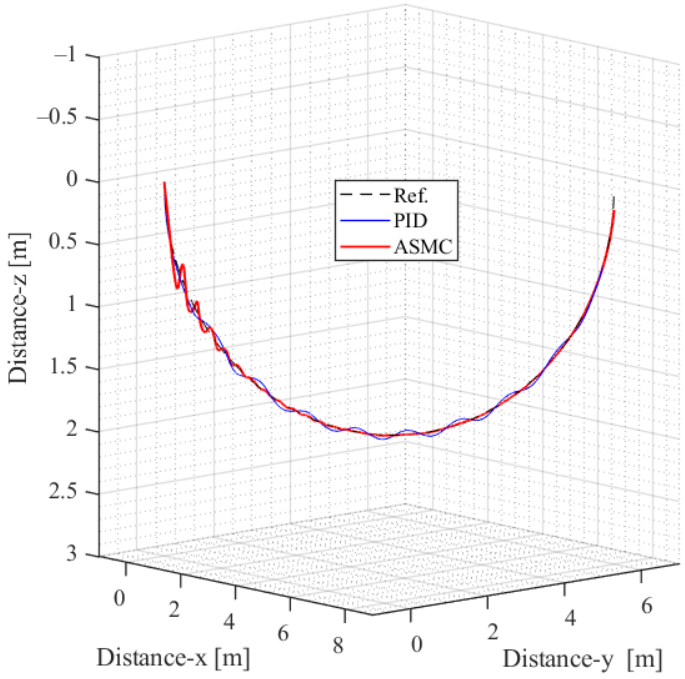


Figure 8. Motion performance of the ROV in the approaching stage.

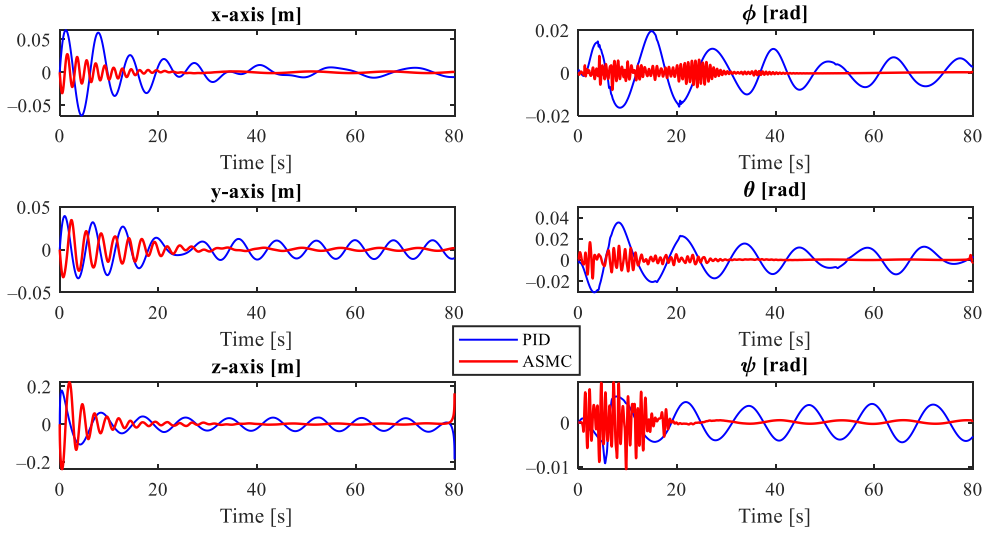
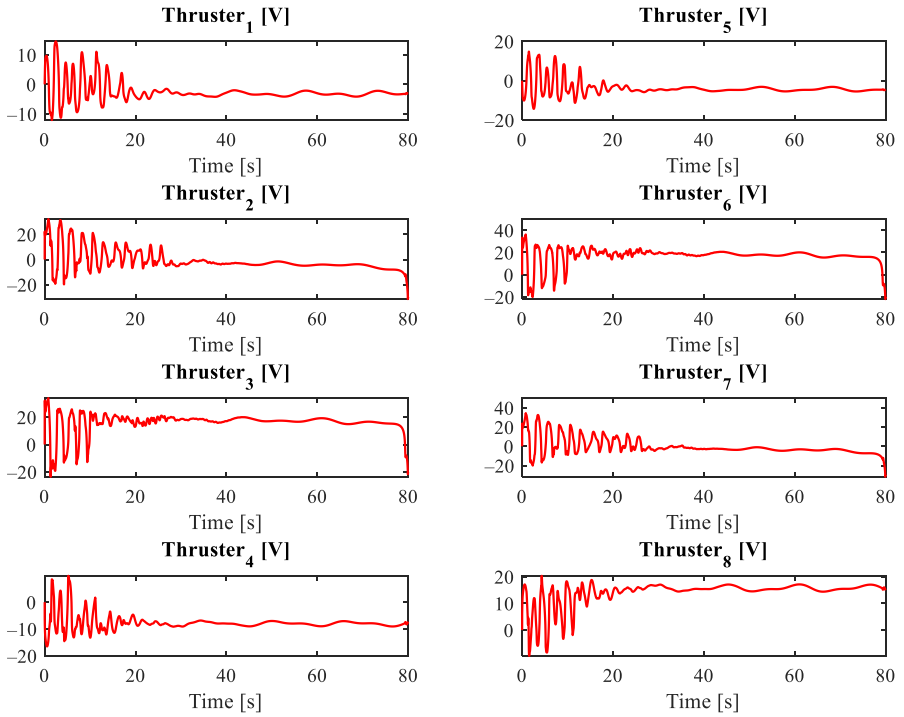
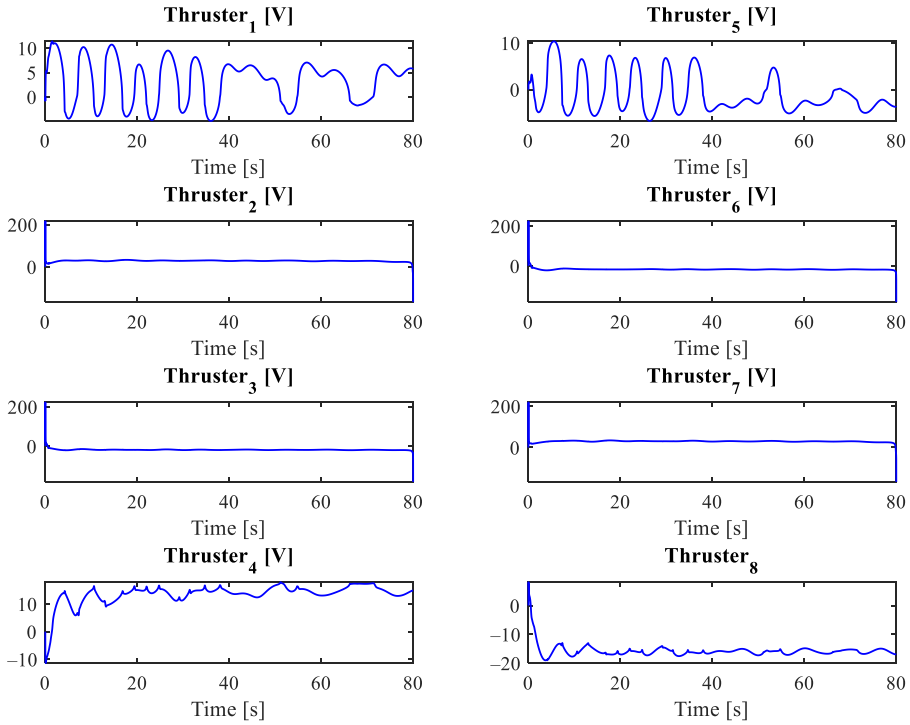


Figure 9. Tracking errors in the approaching stage.



(**a**) The cascade ASMC-PI control



(**b**) The comparative PID-PI control

Figure 10. Control inputs of the ROV in the approaching stage.

5.3. Motion Performance in the Retrieving Stage

The motion performance in the retrieving stage is represented in the same manner as the previous stage. The tracking trajectory, tracking errors and voltage inputs are respectively shown in Figures 11–13. Due to the resistant force and moment of the glider, the motion performance is worse than in the first two stages. For example, the roll and pitch of the ROV controlled by the proposed ASMC-PI cannot converge completely. Fortunately,

the stable motion of the ROV is still maintained. Meanwhile, the effects of the glider on the ROV's motion are significant with the comparative PID-PI controller. It is also worth noting that the requirement of precision tracking is not as critical as in the first two stages. Therefore, the ROV has proved its ability for the glider recovery mission, and the proposed ASMC-PI control system has demonstrated its superiority.

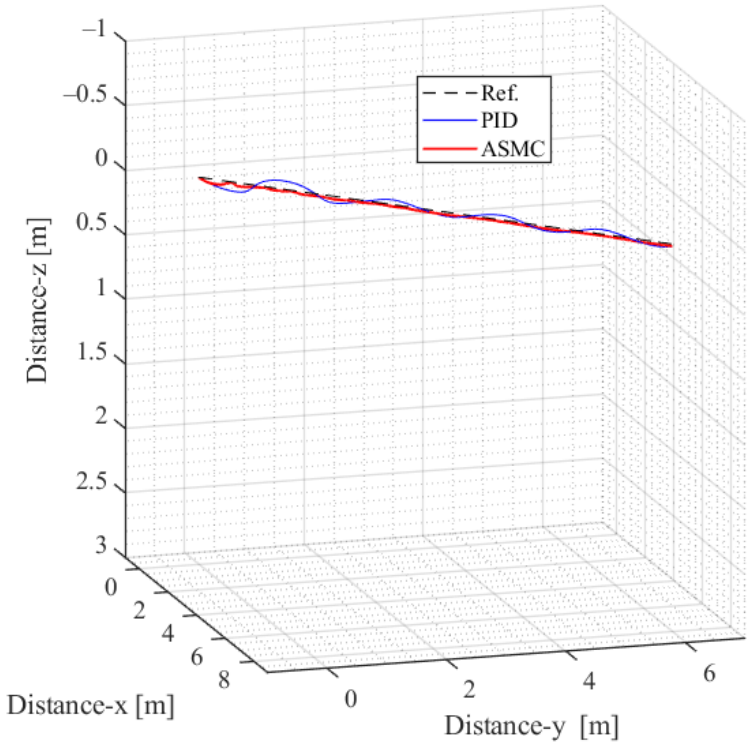


Figure 11. Motion performance of the ROV-glider system in the retrieving stage.

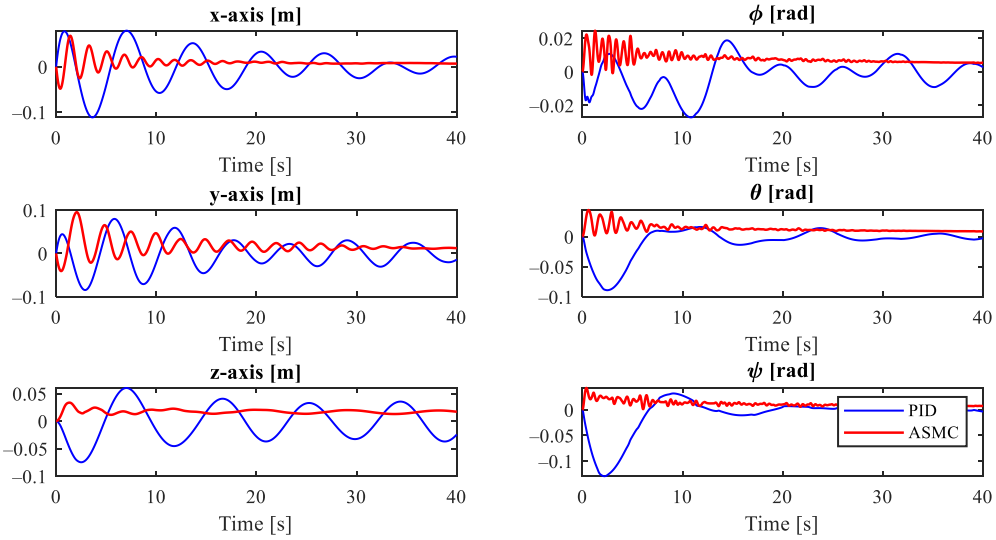
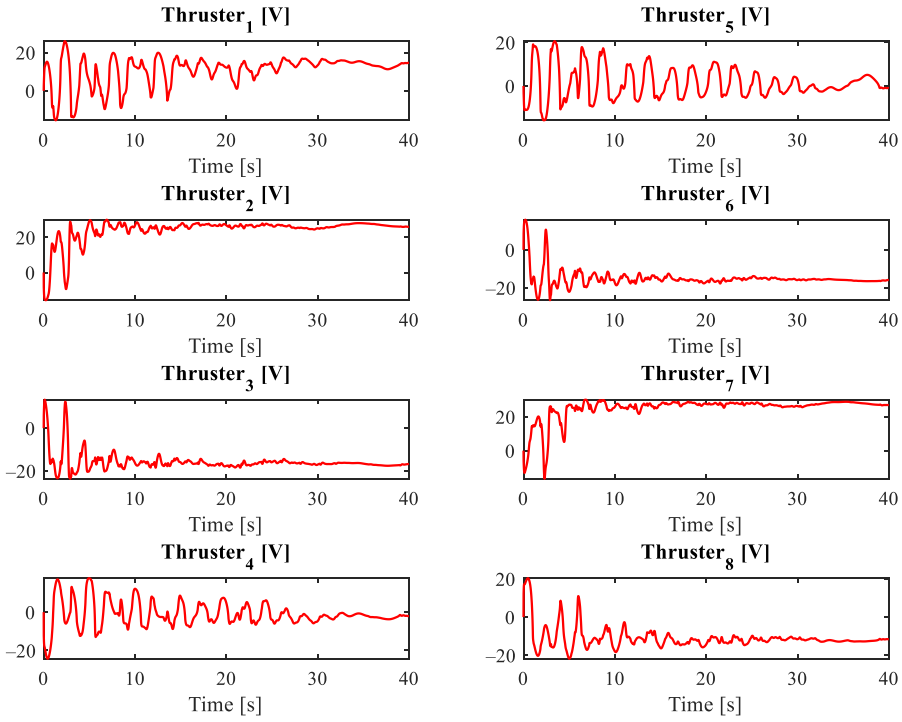
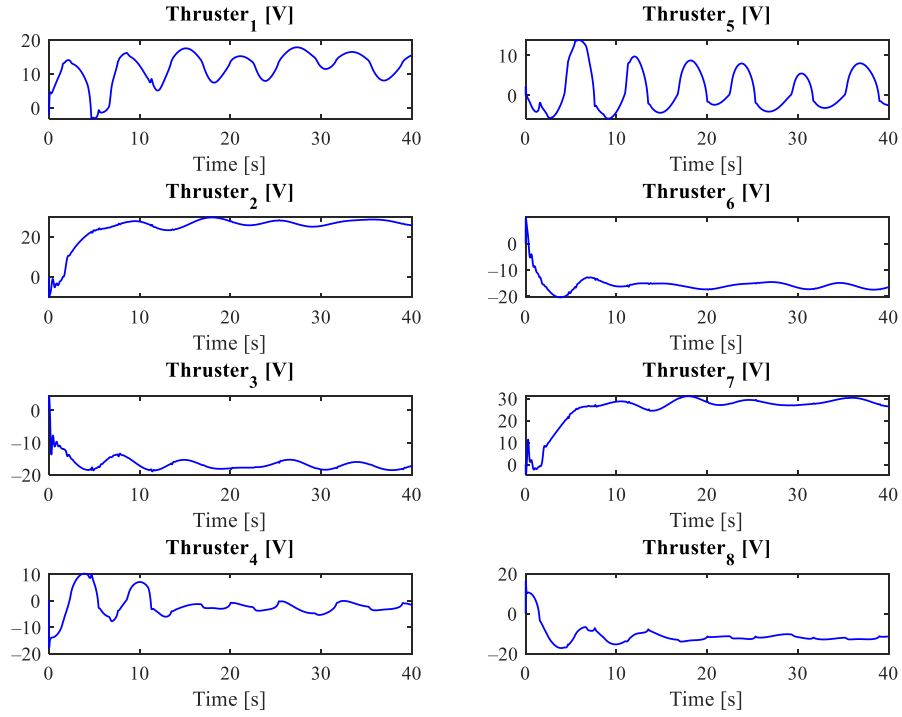


Figure 12. Tracking errors in the retrieving stage.



(**a**) The cascade ASMC-PI control.



(**b**) The comparative PID-PI control.

Figure 13. Control inputs of the ROV in the retrieving stage.

6. Conclusions

In this study, a novel recovery process has been proposed for an underwater glider by using ROV and a motion control system. The ROV is equipped with instruments and capturing mechanisms to perform three successive tasks: approaching, capturing, and retrieving the glider. The cascade ASMC-PI controller has been designed such that a safe and effective recovery is achieved. In order to validate the proposed system, the simulations were conducted in the first and final stages of the recovery process. The simulation results

show that the proposed system achieves high motion performance in the former stage and maintains a robust operation in the latter. In comparison with a cascade PID-PI control system, the proposed system demonstrated its superiority in the recovery process.

For future works, the specifications of the ROV and the glider will shortly be finalized. The experimental system will be fabricated, and experimental studies will be conducted for further evaluation.

Author Contributions: Conceptualization, J.-H.S.; methodology, T.H., Y.-B.K. and M.-T.T.; validation, T.H., M.-T.T. and J.-H.S.; investigation, T.H., M.L., J.L. and M.-T.T.; writing—original draft preparation, T.H. and M.-T.T.; writing—review and editing, T.H., M.-T.T. and J.-H.S.; visualization, T.H. and M.-T.T.; supervision, J.-H.S.; project administration, J.-H.S.; funding acquisition, J.-H.S. All authors have read and agreed to the published version of the manuscript.

Funding: This research was supported by Korea Institute of Marine Science & Technology Promotion (KIMST) funded by the Ministry of Ocean and Fisheries (2020048213, Development of the core technology and establishment of the operation center for underwater gliders).

Institutional Review Board Statement: Not applicable.

Informed Consent Statement: Not applicable.

Data Availability Statement: Not applicable.

Conflicts of Interest: The authors declare no conflict of interest.

References

1. Seaglider: Autonomous Underwater Vehicle. Available online: https://www.apl.washington.edu/project/project.php?id=seaglider (accessed on 2 September 2022).
2. Glider Recovery—Oregon State University. Available online: https://www.flickr.com/photos/oregonstateuniversity/5426475706 (accessed on 2 September 2022).
3. SCIENCE IN THE SEA—Part 3: Gliders Galore! Available online: https://www.bas.ac.uk/blogpost/science-in-the-sea-part-3-gliders-galore/ (accessed on 2 September 2022).
4. Roemmich, D.; Owens, B. The Argo Project: Global Ocean Observations for Understanding and Prediction of Climate Variability. *Oceanography* **2000**, *13*, 45–50. [CrossRef]
5. Hi-Tech Rubber Ducks: Drifters, Gliders and Argo | All at Sea. Available online: https://samspostgrads.wordpress.com/2012/07/06/hi-tech-rubber-ducks-drifters-gliders-and-argo/ (accessed on 12 September 2022).
6. Esteba, J.; Cieslak, P.; Palomeras, N.; Ridao, P. Docking of Non-Holonomic AUVs in Presence of Ocean Currents: A Comparative Survey. *IEEE Access* **2021**, *9*, 86607–86631. [CrossRef]
7. Feezor, M.D.; Yates Sorrell, F.; Blankinship, P.R.; Bellingham, J.G. Autonomous underwater vehicle homing/docking via electromagnetic guidance. *IEEE J. Ocean. Eng.* **2001**, *26*, 515–521. [CrossRef]
8. McEwen, R.S.; Hobson, B.W.; McBride, L.; Bellingham, J.G. Docking Control System for a 54-cm-Diameter (21-in) AUV. *IEEE J. Ocean. Eng.* **2008**, *33*, 550–562. [CrossRef]
9. Howse, S.; Mine-Goldring, M.; Pitcher, M. Underwater glider retrieval using an autonomous surface vehicle. In Proceedings of the OCEANS 2010 MTS/IEEE SEATTLE, Seattle, WA, USA, 20–23 September 2010; pp. 1–8.
10. Watt, G.D.; Roy, A.R.; Currie, J.; Gillis, C.B.; Giesbrecht, J.; Heard, G.J.; Birsan, M.; Seto, M.L.; Carretero, J.A.; Dubay, R.; et al. A Concept for Docking a UUV With a Slowly Moving Submarine Under Waves. *IEEE J. Ocean. Eng.* **2016**, *41*, 471–498. [CrossRef]
11. Guo, J.; Zheng, R.; Yu, X.; Wei, A.; Yang, B. Autonomous underwater vehicle docking system based on wired transmission. In Proceedings of the 2018 WRC Symposium on Advanced Robotics and Automation (WRC SARA), Beijing, China, 16 August 2018; pp. 1–6.
12. Zolich, A.; Johansen, T.A.; Elkolali, M.; Al-Tawil, A.; Alcocer, A. Unmanned Aerial System for deployment and recovery of research equipment at sea. In Proceedings of the 2021 Aerial Robotic Systems Physically Interacting with the Environment (AIRPHARO), Biograd na Moru, Croatia, 4–5 October 2021; pp. 1–8.
13. Recovering Submerged Vehicles Using An ROV. Available online: https://www.deeptrekker.com/resources/recovering-submerged-vehicles (accessed on 2 September 2022).
14. Tarnecki, J.H.; Patterson, W.F. A mini ROV-based method for recovering marine instruments at depth. *PLoS ONE* **2020**, *15*, e0235321. [CrossRef]
15. Sarda, E.I.; Dhanak, M.R. A USV-Based Automated Launch and Recovery System for AUVs. *IEEE J. Ocean. Eng.* **2016**, *42*, 37–55. [CrossRef]
16. Sarda, E.I.; Dhanak, M.R. Launch and Recovery of an Autonomous Underwater Vehicle From a Station-Keeping Unmanned Surface Vehicle. *IEEE J. Ocean. Eng.* **2019**, *44*, 290–299. [CrossRef]

17. Circle, B.N. Underwater mobile docking of autonomous underwater vehicles. In Proceedings of the 2012 Oceans, Hampton Roads, VA, USA, 14–19 October 2012; pp. 1–15.
18. Sarda, E.; Dhanak, M. Unmanned recovery of an AUV from a surface platform manuscript, oceans '13 MTS/IEEE San Diego. In Proceedings of the OCEANS 2013 MTS/IEEE—San Diego: An Ocean in Common, San Diego, CA, USA, 23–27 September 2013; pp. 5–10.
19. Sollesnes, E.; Brokstad, O.M.; Boe, R.K.; Vagen, B.; Carella, A.; Alcocer, A.; Zolich, A.P.; Johansen, T.A. Towards autonomous ocean observing systems using Miniature Underwater Gliders with UAV deployment and recovery capabilities. In Proceedings of the 2018 IEEE/OES Autonomous Underwater Vehicle Workshop (AUV), Porto, Portugal, 6–9 November 2018; pp. 1–5.
20. Mouring, S.E.; Falls, J.; Scharar, T.; Coleman, Z.; Halim, M.A.; Wolf, S.; Arroyo, J.; Zakravsky, S. Design of a recovery system for the SV3 wave glider. In Proceedings of the OCEANS 2017—Anchorage, Anchorage, AK, USA, 18–21 September 2017; pp. 1–6.
21. Rice, J.; Gish, L.A.; Barney, J.; Gawboy, Z.; Mays, B.; Moore, L.; Nickell, A. Design and analysis of an improved Wave Glider recovery system. In Proceedings of the OCEANS 2016 MTS/IEEE Monterey, Monterey, CA, USA, 19–23 September 2016; pp. 1–5.
22. Yan, Z.; Gong, P.; Zhang, W.; Li, Z.; Teng, Y. Autonomous Underwater Vehicle Vision Guided Docking Experiments Based on L-Shaped Light Array. *IEEE Access* **2019**, *7*, 72567–72576. [CrossRef]
23. Liu, S.; Ozay, M.; Xu, H.; Lin, Y.; Okatani, T. A Generative Model of Underwater Images for Active Landmark Detection and Docking. In Proceedings of the 2019 IEEE/RSJ International Conference on Intelligent Robots and Systems (IROS), Macau, China, 3–8 November 2019; pp. 8034–8039.
24. Venkatesh Alla, D.N.; Bala Naga Jyothi, V.; Venkataraman, H.; Ramadass, G.A. Vision-based Deep Learning algorithm for Underwater Object Detection and Tracking. In Proceedings of the OCEANS 2022—Chennai, Chennai, India, 21–24 February 2022; pp. 1–6.
25. Liu, S.; Ozay, M.; Okatani, T.; Xu, H.; Sun, K.; Lin, Y. Detection and Pose Estimation for Short-Range Vision-Based Underwater Docking. *IEEE Access* **2019**, *7*, 2720–2749. [CrossRef]
26. Lee, J.; Choi, Y.; Suh, J. DeConNet: Deep Neural Network Model to Solve the Multi-Job Assignment Problem in the Multi-Agent System. *Appl. Sci.* **2022**, *12*, 5454. [CrossRef]
27. Gianluca, A. *Underwater Robots*, 2nd ed.; Springer Tracts in Advanced Robotics; Springer: Berlin/Heidelberg, Germany, 2006; Volume 2, ISBN 3-540-31752-X.
28. Thor Inge, F. *Guidance and Control of Ocean Vehicles*; John Wiley & Sons: New York, NY, USA, 1994.
29. Boehm, J.; Berkenpas, E.; Shepard, C.; Paley, D.A. Tracking Performance of Model-Based Thruster Control of a Remotely Operated Underwater Vehicle. *IEEE J. Ocean. Eng.* **2021**, *46*, 389–401. [CrossRef]
30. Fossen, T.I.; Blanke, M. Nonlinear output feedback control of underwater vehicle propellers using feedback form estimated axial flow velocity. *IEEE J. Ocean. Eng.* **2000**, *25*, 241–255. [CrossRef]
31. Boehm, J.; Berkenpas, E.; Shepard, C.; Paley, D.A. Feedback-Linearizing Control for Velocity and Attitude Tracking of an ROV with Thruster Dynamics Containing Input Dead Zones. In Proceedings of the 2019 American Control Conference (ACC), Philadelphia, PA, USA, 10–12 July 2019; pp. 5699–5704.
32. Prasanth Kumar, R.; Dasgupta, A.; Kumar, C.S. Robust trajectory control of underwater vehicles using time delay control law. *Ocean Eng.* **2007**, *34*, 842–849. [CrossRef]
33. Hsia, T.C.S. A new technique for robust control of servo systems. *IEEE Trans. Ind. Electron.* **1989**, *36*, 1–7. [CrossRef]
34. Slotine, J.J.E.; Li, W. *Applied Nonlinear Control*; Prentice Hall: Englewood Cliffs, NJ, USA, 1991; ISBN 0130408905.
35. García-Valdovinos, L.G.; Salgado-Jiménez, T.; Bandala-Sánchez, M.; Nava-Balanzar, L.; Hernández-Alvarado, R.; Cruz-Ledesma, J.A. Modelling, Design and Robust Control of a Remotely Operated Underwater Vehicle. *Int. J. Adv. Robot. Syst.* **2014**, *11*, 1. [CrossRef]